NeuroImage 52 (2010) 172–185

Contents lists available at ScienceDirect

NeuroImage

journal homepage: www.elsevier.com/locate/ynimg

Differentiating maturational and aging-related changes of the cerebral cortex by use of thickness and signal intensity

Lars T. Westlye [a,*], Kristine B. Walhovd [a], Anders M. Dale [b,c], Atle Bjørnerud [d,e], Paulina Due-Tønnessen [f], Andreas Engvig [a], Håkon Grydeland [a], Christian K. Tamnes [a], Ylva Østby [a], Anders M. Fjell [a]

[a] Center for the Study of Human Cognition, Department of Psychology, University of Oslo, Norway, PO Box 1094 Blindern, 0317 Oslo, Norway
[b] Multimodal Imaging Laboratory, University of California, San Diego, CA 92103, USA
[c] Departments of Radiology and Neurosciences, University of California, San Diego, CA 92103, USA
[d] Interventional Centre, Oslo University Hospital Rikshospitalet, Sognsvannsveien 20, 0027 Oslo, Norway
[e] Department of Physics, University of Oslo, PO Box 1048 Blindern, 0316 Oslo, Norway
[f] Department of Radiology, Oslo University Hospital Rikshospitalet, Sognsvannsveien 20, 0027 Oslo, Norway

ARTICLE INFO

Article history:
Received 12 January 2010
Revised 16 March 2010
Accepted 19 March 2010
Available online 27 March 2010

Keywords:
Aging
Neurodevelopment
Cerebral cortex
Cortical thickness
MRI T1-weighted signal intensity

ABSTRACT

Cortical thickness decreases from childhood throughout life, as estimated by magnetic resonance imaging (MRI). This monotone trajectory does not reflect the fundamentally different neurobiological processes underlying morphometric changes in development versus aging. We hypothesized that intracortical gray matter (GM) and subjacent white matter (WM) T1-weighted signal intensity would distinguish developmental and age-related changes in the cortex better than thickness. Intracortical GM and subjacent WM signal intensity and cortical thickness was measured across the brain surface in a healthy life span sample ($n = 429$, 8–85 years). We also computed the relaxation rate of T2* (R2*) from multiecho sequences and mapped intracortical GM and subjacent WM values to the surface to delineate age-related variability in R2* and to adjust the T1 signal intensity for possible confounds of accumulated iron. While monotone age-related reductions in thickness were found, both intracortical GM and subcortical WM signal intensity showed inverted U patterns with peaks from eight to approximately 30 years of age. The spatial pattern of intracortical neurodevelopment followed a posterior–anterior gradient, with earliest maturation of occipital visual cortices and most protracted in superior frontal regions. From 50 s and 60 s, substantial signal reductions were observed in several regions, including the insula, cingulate, and inferior temporal gyrus. R2* showed similar patterns but peaked much later than the T1-weighted signal intensity measures. The results are presented as animations yielding detailed depictions of the dynamic regional variability in cortical neurodevelopment and aging and demonstrate that cortical thickness and T1-weighted signal intensity are sensitive to different cortical maturational and aging-related processes.

Introduction

Delineating normal life span development of the cerebral cortex provides indispensible knowledge informing the interpretation of the deviating courses related to developmental and age-related diseases (Tau and Peterson, 2010). Alterations in cortical volume and thickness have been mapped *in vivo* in development (Giedd et al., 1999; Gogtay et al., 2004; Shaw et al., 2008; Sowell et al., 2003, 2004; Tamnes et al., 2010) and aging (Fjell et al., 2009; Good et al., 2001; Jernigan et al., 2001; Raz et al., 2004; Salat et al., 2004; Westlye et al., 2009b) using magnetic resonance imaging (MRI). Accumulating evidence is converging on decreases in cortical thickness and volume from late childhood. Although the neurobiological underpinnings of the morphometric changes are not established, it is likely that fundamentally different processes induce cortical thinning in development and the atrophy seen in adulthood (Sowell et al., 2003). The maturational cortical thinning may be caused by regressive use-dependent selective synapse elimination (Bourgeois and Rakic, 1993; Huttenlocher and Dabholkar, 1997) in combination with progressive proliferation of myelin into the neuropil (Shaw et al., 2008; Sowell et al., 2001; Yakovlev and Lecours, 1967). These processes refine local and distributed network connectivity and enhance the efficiency and synchronicity of signal transmission (Tau and Peterson, 2010). Cortical thinning is thus regarded an early maturational marker. In contrast, adult cortical thinning has been attributed to degenerative shrinkage of large neurons (Terry et al., 1987), loss of myelinated axonal fibers (Nairn et al., 1989), deafferentation (Bertoni-Freddari et al., 2002), and reduction in synaptic density (Morrison and Hof, 1997).

Cortical thickness fails to distinguish between maturational and aging-related neurobiological processes. However, by mapping

* Corresponding author. Fax: +47 22845001.
E-mail address: l.t.westlye@psykologi.uio.no (L.T. Westlye).

1053-8119/$ – see front matter © 2010 Elsevier Inc. All rights reserved.
doi:10.1016/j.neuroimage.2010.03.056

intracortical T1-weighted signal intensity, we may differentiate the neurobiological processes associated with development from those associated with aging. T1-weighted signal intensity reflects the underlying tissue proton relaxation times, which is related to degree of myelination (Barbier et al., 2002; Clark et al., 1992; Eickhoff et al., 2005; Walters et al., 2003). Signal intensity alterations may provide an independent biomarker of structural alterations in development, aging, and disease (Salat et al., 2009; Westlye et al., 2009b).

The aim of this study was to track cortical GM and subcortical WM development and aging by surface-based mapping of cortical and subcortical T1-weighted signal intensity and R2* as well as cortical thickness in 429 participants aged 8–85 years. We anticipated signal intensity increases from childhood through adolescence and decline in the latter half of life. Since signal intensity is related to tissue myeloarchitecture, we expected cortical trajectories similar to those demonstrated in white matter microstructural maturation, with increases well into adulthood (Lebel et al., 2008; Westlye et al., in press). This stands in contrast to the monotone cortical thinning from childhood. In line with evidence of a maturational posterior–anterior gradient (Gogtay et al., 2004), we expected early maturation of sensorimotor areas including visual cortices, followed by association areas and last in higher-order frontal and posterior parietal cortices. Following an inverse ontogenetic course in aging (Courchesne et al., 2000; Raz, 2000), we expected earliest decline in frontoparietal cortices and latest in sensorimotor areas.

Several biophysical variables influence the T1-weighted signal. Changes in T2 and T2* relaxation secondary to iron depositions may modulate the T1-weighted signal intensity, even on strongly T1-weighted acquisitions like the MP-RAGE sequence used in the present study. Therefore, possible confounding effects of bioaccumulated iron, with consequent reduction in T2* relaxation times, were controlled by including T2* relaxation rate (R2*) computed from multiecho sequences as additional covariates in the statistical models. Since R2* also may index relevant age-related biophysical variability, we delineated the age trajectories for intracortical GM and subjacent WM R2* across the life span.

Materials and methods

Subjects

The sample was drawn from the first wave of two ongoing longitudinal research projects at the Center for the Study of Human Cognition at the University of Oslo, namely, *Neurocognitive Development* and *Cognition and Plasticity through the Lifespan* and is overlapping with the sample in Westlye et al. (in press). The studies were approved by the Regional Ethical Committee of Southern Norway (REK-Sør). Participants were recruited through newspaper ads and among students and employees at the University of Oslo and from local schools. Further details regarding recruitment and enrolment are given elsewhere (Tamnes et al., 2010; Westlye et al., 2009a). Written informed consent was obtained from all participants from 12 years of age and from parent/guardian for participants below 18 years of age. Oral informed consent was given by participants under 12 years of age. A total of 429 healthy participants (54.8% females) aged 8–85 years (mean: 41.6 years, SD: 22.0 years) were included. Demographics are summarised in Table 1. Independent-samples *t*-test revealed no effect of sex on age (females: 42.0 years (SD = 21.2 years), males: 41.1 years (SD = 22.9 years), $P > 0.67$). All subjects were right-handed native Norwegian speakers. Subjects with history of neurological or psychiatric conditions thought to influence cerebral functioning, including clinically significant stroke, serious head injury as well as use of psychoactive drugs within the last 2 years were excluded. All participants above 20 years of age scored <16 on Beck Depression Inventory (BDI) (Beck and Steer, 1987) and subjects above 40 years of age scored ≥26 on Mini Mental State Examination (MMSE) (Folstein et al., 1975). General cognitive abilities were assessed by Wechsler Abbreviated Scale of Intelligence (WASI) (Wechsler, 1999). Mean full-scale IQ for the entire sample was 113.4 (range: 82–145, SD = 9.9). All subjects' MRI scans were examined by a neuroradiologist and deemed free of significant anomalies. A total of 437 subjects were enrolled in the studies. For the current analyses, four subjects were excluded due to subject motion artefacts, one was excluded due to age (>90 years, which created a gap of missing data points on the continuous age scale), two were excluded after radiological evaluation, and one was excluded due to missing neuropsychological assessment, yielding a final sample of 429 subjects.

Table 1
Sample descriptives by age group and total.

Age group (years)	*n*	Females, *n* (%)	FIQ,[a] mean (SD)	MMS,[b] mean (SD)	Years education,[c] mean (SD)	Age (years), mean (SD)
8–9	20	9 (45.0)	105.0 (11.6)	n.a.	n.a.	9.0 (0.5)
10–19	88	46 (52.3)	109.8 (10.6)	n.a.	n.a.	15.0 (2.8)
20–29	55	28 (50.9)	112.5 (7.1)	n.a.	15.1 (1.9)	24.0 (2.6)
30–39	36	22 (61.1)	115.2 (8.6)	n.a.	17.3 (2.4)	34.6 (2.8)
40–49	38	24 (63.2)	115.7 (7.0)	29.5 (0.6)	15.3 (2.0)	44.9 (3.0)
50–59	78	46 (59.0)	112.8 (7.7)	29.2 (0.8)	15.2 (2.2)	54.2 (2.8)
60–69	66	37 (56.1)	116.0 (10.5)	29.1 (0.9)	16.1 (3.2)	64.2 (2.7)
70–79	35	18 (51.4)	118.9 (10.3)	28.9 (1.2)	15.4 (3.6)	72.5 (2.5)
80–85	13	5 (38.5)	117.7 (14.6)	28.5 (0.8)	14.8 (2.4)	82.0 (1.6)
Total	429	235 (55.3)	113.4 (9.9)	29.1 (0.9)	15.6 (2.6)	41.6 (22.0)

n.a.: not available.
[a] Full-scale IQ (FIQ) was estimated from the WASI (Wechsler, 1999) subtests matrices, block design, vocabulary, and similarities. For a subset of 39 subjects, only matrices and vocabulary were available.
[b] MMS (Folstein et al., 1975) scores not available for subjects below 40 years of age.
[c] Years of education was not estimated for subjects below 20 years. Most subjects between 20 and 30 years of age were recruited among university students, and years of education were calculated as number of years completed at time of assessment.

MRI acquisition

Imaging was performed using a 12-channel head coil on a 1.5-T Siemens Avanto (Siemens Medical Solutions, Erlangen, Germany). The pulse sequence used for morphometric and signal intensity analyses was a T1-weighted magnetization prepared rapid gradient echo (MP-RAGE). TR/TE/TI/FA = 2400 ms/3.61 ms/1000 ms/8°, matrix = 192 × 192, field of view = 240. Each volume consisted of 160 sagittal slices with voxel size of 1.25 × 1.25 × 1.20 mm. The pulse sequence used to compute R2* was a multiecho fast low angle shot (ME-FLASH) with eight different TEs: 1.85, 3.85, 5.85, 7.85, 9.85, 11.85, 13.85, and 15.85 ms. Common parameters across echoes were TR = 20 ms, FA = 5°, matrix = 256 × 256, and field of view = 256. Each volume consisted of 176 sagittal slices with isotropic voxels with a slice thickness of 1 mm. Multiecho data were available for 414 (96.5%) of the participants.

MRI processing

Raw data sets were transferred to Linux workstations for processing and analyses at the Neuroimaging Analysis Lab, Center for the Study of Human Cognition, University of Oslo, with additional use of computing resources from the Titan High Performance Computing facilities (http://hpc.uio.no/index.php/Titan) at the University of Oslo. All data sets were processed and analysed with FreeSurfer (http://surfer.nmr.mgh.harvard.edu/). Estimates of cortical thickness were obtained by reconstructing representations of the WM/GM boundary and the cortical surface (Dale et al., 1999; Dale and Sereno, 1993; Fischl et al., 1999b) and then calculating the distance between these surfaces at each vertex across the cortical mantle.

The thickness maps are created using spatial intensity gradients across tissue classes and are not simply reliant on absolute signal intensity. The maps are not restricted to the voxel resolution of the raw data and are capable of detecting submillimeter differences between groups (Fischl and Dale, 2000). The method has been validated using histology and MRI (Kuperberg et al., 2003; Rosas et al., 2002). The signal intensity analyses were performed in line with a previous publication (Westlye et al., 2009b). Briefly, volumes used for signal intensity mapping were resampled to $1\times1\times1$ mm, zero padded to $256\times256\times256$ dimension, motion-corrected, and, where available, averaged over multiple acquisitions yielding one high SNR volume. No high- or low-frequency intensity normalization was performed on the volumes from which intensity values were sampled. Intensity normalization (i.e., where the tissue classes are individually scaled to normalized distributions) could influence the present results by assuming indifferent mean intensities for each tissue class across subjects.

Cortical T1-weighted signal intensity was sampled towards the pial surface at a distance of 1.0 mm from the WM/GM boundary (white surface) at every vertex across the brain surface. WM signal intensity was sampled towards the center of the gyri at a distance of 2.0 mm from the white surface. Signal intensities in MP-RAGE images cannot be assumed to be constant across participants for the same underlying relaxation parameters due to session- and participant-specific optimization procedures performed during MR acquisition. Signal intensity values were therefore normalized with respect to cerebrospinal fluid (CSF) intensity to correct for possible intersubject variations in scaling factors (Westlye et al., 2009b). An automated subcortical segmentation procedure implemented in FreeSurfer (Fischl et al., 2002, 2004a) was used to extract intensity values from lateral ventricular CSF.

The segmentation procedure automatically assigns a neuroanatomical label to each voxel in the MRI volume based on probabilistic information automatically estimated from a manually labeled training set (Fischl et al., 2002). The original training set included healthy subjects aged 18–87 years and Alzheimer's disease patients aged 60–87 years. The voxel classification employs a registration procedure that is robust to anatomical variability, including the ventricular enlargement typically associated with aging, and has previously been shown to be comparable in accuracy to manual labeling (Fischl et al., 2002, 2004a). An atlas-based normalization procedure shown to increase segmentation robustness and accuracy across scanner platforms (Han and Fischl, 2007) was used. Voxels labeled by FreeSurfer as belonging to the choroid plexus were not included in the ventricle segments used in the normalization. To minimize partial voluming of periventricular brain tissue, the ventricle segments were eroded by 2 voxels before signal intensity calculation.

Ventricle signal intensity was chosen as reference for the MP-RAGE signal intensity values because we expected less age dependency in the ventricles compared to, e.g., subcortical structures. Immediate subjacent WM has previously been used as reference for cortical GM signal intensity values (Salat et al., 2009). However, this was not an optimal approach in the present study since the main aim was to track the absolute and not relative changes of both the cortical GM and subcortical WM. It is not likely that surface-based measures of cortical GM and subjacent WM changes are independent markers of life span structural alterations. For the same reasons, we did not reference the surface mapped measures to other subcortical GM or WM structures.

Linear regression with ventricle signal intensity as dependent variable and sex, age and age^2 as independent variables yielded no significant effects of sex ($t=1.57$, $p=.12$) or age ($t=0.12$, $p>.90$) but a moderate yet significant negative effect of age^2 ($t=-2.01$, $p<.05$), indicating an inverse U curve through the life span. However, adding estimated intracranial volume (ICV) (Buckner et al., 2004) as an additional covariate removed the age^2 effect and revealed a significant unique effect of ICV on lateral ventricle intensity ($t=4.065$, $p<.001$). Thus, ICV was included as a covariate in the linear regressions testing for age effects on intracortical MP-RAGE signal intensity in selected neuroanatomical regions of interest. Before the surface-based analyses, we removed the variance related to ICV from each subject's T1-weighed signal intensity maps by means of vertexwise linear regressions. Thus, all surface-based T1-weighted signal intensity analyses were performed on residualized maps after removing the effects of ICV. The spatial distribution of the effects (t scores) of ICV on cortical GM signal intensity covarying for sex, age, age^2, and cortical thickness across the life span is shown in Supplementary Fig. 1.

R2* volume maps were calculated in Matlab by linear fitting to the log-transformed signal intensity across multiple echoes (TEs). The resulting R2* volumes were then spatially aligned to the T1-weighted volumes (Greve and Fischl, 2009) and vertexwise R2* values were mapped to the surface as described above.

All surface maps were smoothed using a circularly symmetric Gaussian kernel across the surface with a full-width at half-maximum (FWHM) of 15 mm and averaged across participants using a nonrigid high-dimensional spherical averaging method to align cortical folding patterns (Fischl et al., 1999a). This provides accurate matching of morphologically homologous cortical locations on the basis of each individual's anatomy, resulting in a measure of interest for each subject at corresponding vertices. All vertices were thus represented with a value of cortical thickness, intracortical GM, and subcortical WM T1-weighted signal intensity as well as intracortical GM and subcortical WM R2*. The surface was divided into 33 gyral-based areas in each hemisphere (Desikan et al., 2006; Fischl et al., 2004b), and measures of interest were averaged within these labels. Distributed ROIs were selected for statistical testing.

The surface reconstruction and segmentation are run automatically but require manual supervision of the accuracy of the spatial registration and tissue segmentations. The types of errors that most often prompted user intervention were insufficient removal of nonbrain tissue adjacent to the cortex. All volumes were visually checked for accuracy, and segmentation errors were manually corrected by trained operators. Minor manual edits were performed on most (>80%) subjects, usually restricted to removal of nonbrain tissue orbitofrontally included in the cortical surface.

Due to subject motion artefacts, one MP-RAGE was excluded for 25 children ranging 8–16 years of age (10 girls of mean age 10.1 years and 15 boys of mean age 11.1 years, in total mean age 10.7 years, SD = 2.0). To ensure that the number of structural scans did not confound our results, we reran all regressions with number of scans as an additional fixed factor. In no instances did these analyses yield significant or trend effects of number of scans on signal intensities. The main analyses were thus performed without adjusting for number of scans.

Possible confounding effects of bioaccumulated iron, with consequent reduction in T2* relaxation rate (R2*), were controlled statistically by including R2* calculated from multiecho sequences as vertexwise covariates in the statistical models.

Statistical analyses

We expected nonlinear and nonmonotonic age trajectories for T1-weighted signal intensity. Thus, cortical and WM signal intensities were first fitted with GLMs testing the effects of age^2 to evaluate the suitability for peak estimation. Sex and age were included as covariates. Since we previously have shown monotone thinning from the earliest age sampled (Tamnes et al., 2010), we did not estimate peaks for cortical thickness.

Next, every vertex with its corresponding measure of interest was fitted by means of robust locally weighted polynomial regression (rLOESS) as a function of age (Cleveland and Devlin, 1988). Age at the maximum estimated value was mapped back to the surface. Similarly, timing of age-related cortical deterioration defined as age when T1-

weighted signal intensity value equalled 50% of the difference between maximum value and value at maximum age was mapped to the surface. This enabled dynamic spatiotemporal mapping of neurodevelopment and age-related cortical deterioration. We have recently employed a similar procedure for mapping life span WM changes using diffusion tensor imaging (DTI) (Westlye et al., in press). The vertexwise rLOESS fitting was done using custom Matlab routines. rLOESS was used to avoid enforcing a common parametric function on the full data set, and thus also avoiding making any priors with respect to curve shape. Since rLOESS function does not represent a specific model expression, no formal tests of significance were implemented.

As the surface-based mappings do not provide information regarding curve shapes, mean cortical GM and subcortical WM signal intensity values and cortical GM R2* from eight selected neuroanatomical ROIs (superior frontal gyrus, medial orbitofrontal cortex, rostral middle frontal, paracentral, superior parietal, inferior temporal gyrus, isthmus cingulate, and pericalcarine) were smoothed using rLOESS and plotted with cortical thickness as a function of age. Note that all curves were fitted to the residuals after removing ICV-related variance by means of linear regressions.

We supplemented the curve fitting and peak estimations with statistical tests of linear effects by dividing the sample into three age groups pragmatically chosen based on visual inspection of the estimated curves and an attempt to keep sample size approximately similar across groups: 1) 8–30 years ($n=163$), 2) 31–57 years ($n=139$), and 3) 58–86 years ($n=127$). Linear effects of age on thickness and intracortical GM and subjacent WM T1-weighted signal intensity and cortical GM R2* in each age group were tested with GLMs at each vertex while controlling for sex. Further, to explore the dependence of cortical thickness to signal intensity alterations, effects of age on cortical thickness were tested while allowing cortical GM and subcortical WM T1-weighted signal intensity to covary on a vertex-by-vertex basis. Similarly, we included cortical thickness as an additional vertexwise covariate in the signal intensity analyses to ensure that the age-related variance in signal intensity was not explained by concurrent cortical thinning. We also correlated the vertexwise values of cortical thickness and intracortical GM signal intensity in the three age groups to explore possible age interactions in the relationships between the cortical GM measures. Also, quantitative R2* values were included as vertexwise covariates in the signal intensity analyses to control for possible confounding effects of iron depositions.

The statistical p maps were thresholded at $p<.01$. This threshold was in all instances more conservative than estimated 5% false discovery rate (FDR) (Genovese et al., 2002) but was chosen consistently instead of the suggested FDR values to aid comparison between measures.

Effects of age, age^2, sex, and ICV on cortical GM and WM T1-weighted signal intensity were tested in select ROIs using multiple linear regressions. Peaks estimated by rLOESS and ordinary least square (OLS) regressions with age^2 as independent variable are reported for comparison with other studies.

Results

Quadratic effects of age

Supplementary Fig. 2 shows statistical p maps ($p<.01$) from GLMs testing for quadratic effects of age on intracortical GM and subcortical WM T1-weighted signal intensity and intracortical GM R2* while regressing out linear effects of age and sex. Widespread negative quadratic effects (inverse U curves) of age were observed across measures.

Intracortical GM T1-weighted signal intensity

Fig. 1A shows color-coded surface mappings of the timing of maximum cortical GM T1-weighted signal intensity (after removal of ICV-related variance per vertex). Occipital areas peaked within the earliest age sampled (<8 years), while frontal areas, including superior frontal, rostral middle frontal, and caudal middle frontal gyri, showed a protracted development into the late 20 s or early 30 s. Fig. 1B depicts the regional timing of the age-related intracortical GM signal intensity decline defined as the age when signal intensity values dropped below 50% of the difference between estimated maximum value and estimated value at maximum age. Insula,

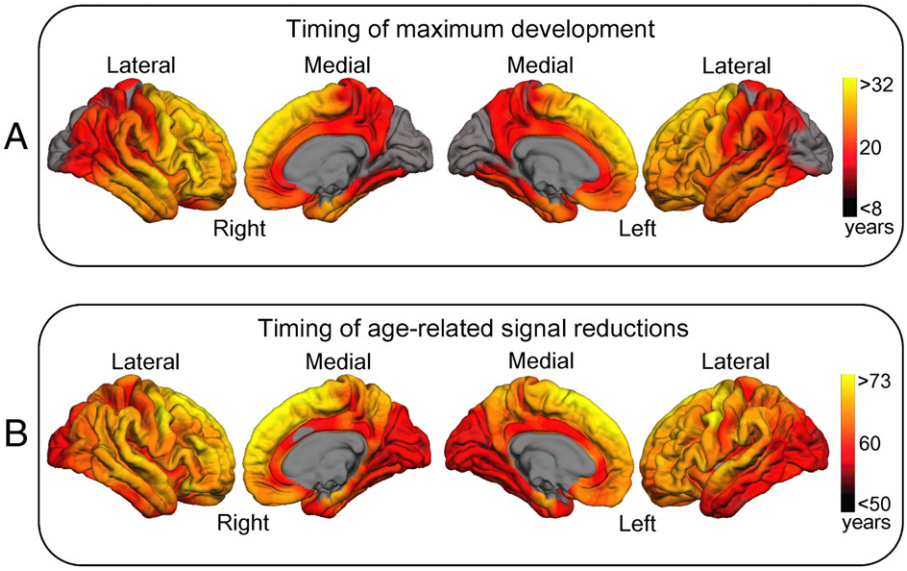

Fig. 1. Timing of life span intracortical GM T1-weighted signal intensity milestones. A) Timing of maximum T1-weighted signal intensity mapped to the surface. A posterior–anterior gradient is seen, with later peaks observed in anterior areas. No areas peaked later than ~31 years. Grey areas peaked earlier than the age range sampled (< 8 years). Time-lapse movies of the spatiotemporal dynamics are provided in Supplementary Movies 1/2. B) Timing of age-related intracortical GM signal decay as indexed by age when reaching the value of 50% of the difference between maximum T1-weighted signal intensity value and estimated value at maximum age. Time-lapse movies of the spatiotemporal dynamics are provided in Supplementary Movies 3/4. The analyses were performed on the residuals after removing variance related to ICV. The medial wall including corpus callosum was excluded.

occipital areas, dorsal cingulate, and inferior temporal gyri were the first regions to approach the threshold, while superior frontal and central gyri were among the last.

Supplementary Movies 1 and 2 show the timing of peak intracortical GM T1-weighted signal intensity in the lateral/medial and dorsal/ventral views, respectively. Supplementary Movies 3 and 4 show the timing of the age-related cortical deterioration in the lateral/medial and dorsal/ventral views, respectively. Fig. 2A depicts snapshots from Supplementary Movies 1 and 2. Green color indicates regions having reached the maturational peak. The pattern suggests a posterior–anterior gradient of neurodevelopment, with the latest maturation seen in superior anterior areas with peaks around 30 years of age. Fig. 2B shows snapshots corresponding to Supplementary Movies 3 and 4. Red color denotes areas falling below 50% of the total signal attenuation from estimated peak. Few areas reached the threshold before 60 years of age, approximately 30 years after estimated maturational peak. Earliest deterioration was seen in the right dorsal cingulate cortex (~54 years) followed by medial occipital areas (~ 60 years) and the remains of the cingulate cortex (~62–66 years). Latest deterioration was observed in superior frontal areas, which showed a relative perseveration until the late 60s and early 70s.

Fig. 3 depicts rLOESS estimated trajectories for intracortical GM T1-weighted signal intensity (residuals after removing ICV-related variance) and thickness in eight ROIs in the left hemisphere. While the cortices showed monotone thinning from 8 to 85 years, intracortical signal intensity in general showed evidence of early maturational periods approaching peak before slow but accelerating decreases in middle adulthood and senescence. Note that for most ROIs including the superior frontal gyrus, medial orbitofrontal cortex, rostral middle frontal gyrus, paracentral, and isthmus cingulate, approximately half of the estimated life span cortical thinning is done when the T1-weighted signal intensity reaches its maximum value. Also, the thickness curves for medial orbitofrontal cortex, paracentral, superior parietal, inferior temporal, and pericalcarine indicate a temporary decelerating thinning from approximately late 20s to the early 40s. Results from multiple linear regressions with cortical GM signal intensity (not residualized for ICV) as dependent variable and age, age^2, ICV, and sex as independent variables for various neuroanatomical ROIs in the left hemisphere are summarized in Table 2, which also shows the age at rLOESS- and OLS-estimated peaks for each ROI.

For comparison and validation, Supplementary Fig. 3 shows the rLOESS-estimated age trajectories for intracortical GM MP-RAGE signal intensity values used in the present analyses together with the MP-RAGE signal intensity sampled from volumes corrected for intensity nonuniformity for various ROIs. The correction was performed using nonparametric nonuniform intensity normalization (N3) by means of the MINC tool 'nu_correct' (Sled et al., 1998) embedded within the FreeSurfer stream with the default smoothing distance $d = 200$ mm. The trajectories were highly parallel and showed the same general pattern of increasing signal intensity during maturation and decreasing in senescence. Supplementary Fig. 4 shows the spatial distribution of the vertexwise correlations between the two volumes. The correlations were, in general, high (Pearson's $r > .08$) across the surface and slightly higher in posterior compared to anterior areas. Note that the rLOESS-estimated maturational signal intensity increases in the superior frontal gyrus, and the isthmus cingulate was less clear in the nonuniformity corrected than in the noncorrected values. These areas also showed weaker correlations between values than other regions.

Effects of age on cortical thickness and intracortical GM T1-weighted signal intensity in different age groups

Fig. 4 shows spatial p value distributions from GLMs testing linear effects of age on thickness in three different age cohorts, before and after including intracortical GM and subcortical WM T1-weighted signal intensity (residualized for ICV) as vertexwise covariates. The statistical threshold ($p < .01$) was regarded more conservative than the estimated 5% FDR threshold (Genovese et al., 2002) in all instances with effects. As indicated by the ROI curves shown in Fig. 3, cortical thinning was most significant and widespread in the youngest group, followed by relatively moderate thinning in the adult groups. Age-related thinning in the middle-aged cohort was strongest bilaterally in frontal areas, including superior frontal gyri and lateral orbitofrontal cortices and in the cuneus and lateral occipital gyri. In the elderly group, thinning was seen bilaterally in inferior parietal, supramarginal, middle frontal gyri, and the temporal lobes, including superior and middle temporal gyri, fusiform, and entorhinal cortices. Minor areas of cortical thickening were observed bilaterally in the insula and the caudal anterior cingulate cortices.

The effect of including cortical T1-weighted signal intensity in the models was negligible in the youngest group. Age effects decreased slightly in the middle-aged group, but the regional pattern remained unchanged. However, little residual cortical thinning was found in the

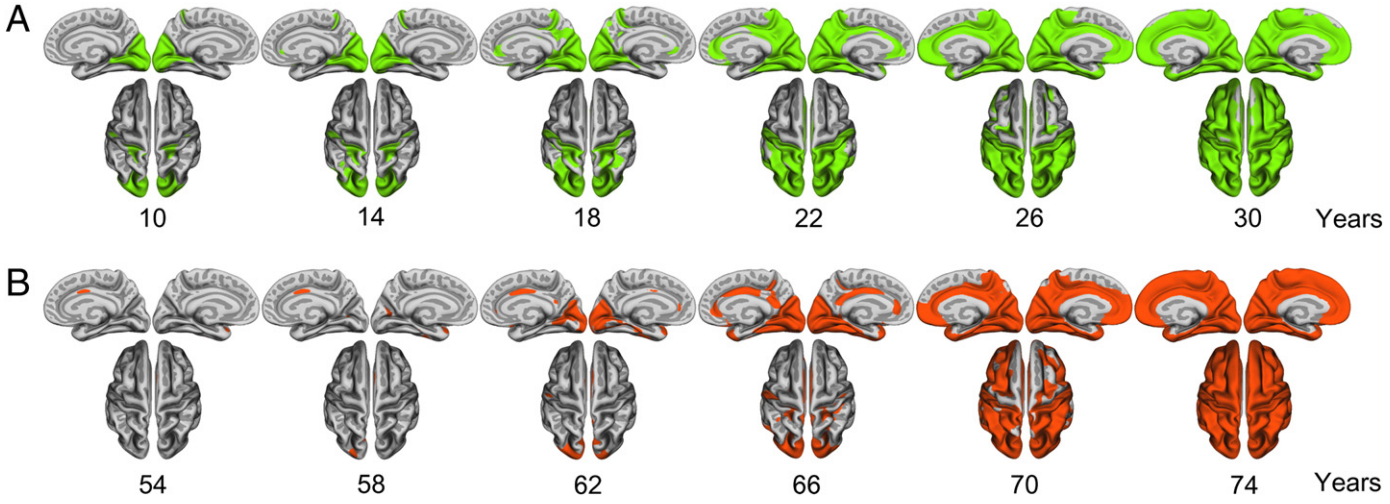

Fig. 2. Spatiotemporal pattern of intracortical GM life span alterations. A) Vertexwise mapping of age at maximum cortical development as indexed by intracortical GM T1-weighted signal intensity peak (green). B) Timing of age-related cortical deterioration as indexed by the age when intracortical GM signal intensity value dropped below 50% of the difference between estimated maximum value and estimated value at maximum age (red). The numbers denote age in years at which the snapshots were taken.

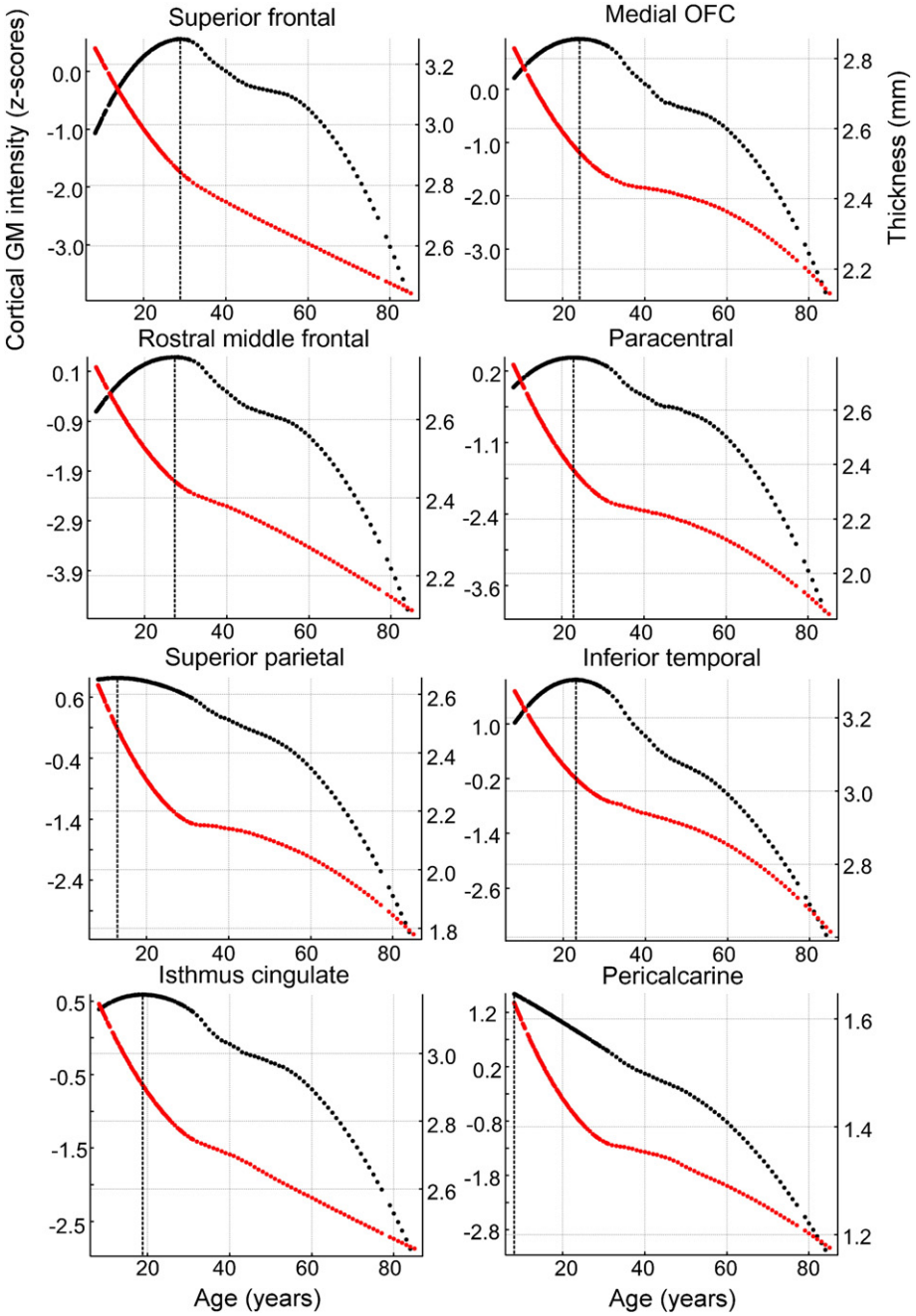

Fig. 3. Intracortical GM T1-weighted signal intensity and thickness through the life span. rLOESS estimated curves for cortical signal intensity (left *y*-axes, black dots) and cortical thickness (right y-axes, red dots) in selected ROIs plotted as a function of age. Vertical dotted lines mark the rLOESS-estimated peaks of signal intensity. Residuals after removing the ICV-related variance were used for the intensity analysis.

oldest group after including cortical GM T1-weighted signal intensity as a covariate. Residual thinning was seen in the anterior medial and lateral temporal lobes. Areas of thickening were less affected. Including subcortical WM T1-weighted signal intensity as an additional covariate slightly increased the estimated effects of age on thickness in all groups compared to when only including cortical GM intensity. Compared to thickness analysis alone, adding cortical GM and subcortical WM T1-weighted signal intensity as covariates increased the effects of age in the youngest group, especially in areas encompassing the precentral gyri. In the middle-aged group, increased effects were seen in several areas, including superior frontal gyri and lateral prefrontal cortices. In the elderly group, slightly decreased *p* values were observed in the lateral temporal lobes and the medial prefrontal cortices.

Fig. 5 shows the effects of age on intracortical GM T1-weighted signal intensity (*z*-scores after removing ICV-related variance) before and after including cortical GM R2* and cortical thickness as vertexwise covariates. As indicated by the ROI analyses, positive effects of age on intracortical GM T1-weighted signal intensity were found in the youngest group, particularly in frontal areas, including the superior frontal gyri, and medial and lateral parts of the temporal lobes. The effects of age in the middle-aged group were negligible, while age effects in the elderly group were strongly negative across most of the surface. Strongest decreases were seen in parietal and medial occipital and temporal and frontal areas. The effects of regressing out intracortical GM R2* were small across groups but slightly larger in the youngest compared to the other groups. The regional patterns remained unchanged, although *p* values were

slightly increased. Including cortical thickness as an additional vertexwise covariate increased the age variance in the youngest group, especially in superior frontal and parietal areas. The age variance decreased slightly in the oldest group but was still significant across almost the entire surface except parts of the medial and lateral temporal lobes and the medial superior frontal gyri.

Fig. 6 shows the results from the surface based correlation analyses between cortical thickness and intracortical GM signal intensity. The results showed no or small correlations in the youngest group, moderate positive correlations in the middle-aged group, and stronger positive correlations in the oldest group. These results support the view that the relations between the different cortical GM measures are not uniform across the life span.

Subcortical WM T1-weighted signal intensity

Results from multiple linear regressions with subcortical WM signal intensity (not residualized for ICV) as dependent and age, age^2, ICV, and sex as independent variables for various ROIs are summarized in Table 3. Supplementary Fig. 5 depicts regional timing of maximum WM T1-weighted signal intensity, Supplementary Fig. 6 depicts ROI-based rLOESS curve fittings, and Supplementary Fig. 7 depicts linear effects of age on subcortical WM T1-weighted signal intensity in different age groups. In the surface-based analyses, residualized values after removing ICV-related variance from the WM T1-weighted signal intensity were used. Briefly, the results were similar to those found for cortical values but with some notable differences. Although the pattern revealed an posterior–anterior gradient, it was less clear than for the cortical GM analyses, and while early myelinating regions, including the visual occipital areas peaked early, they still exhibited a protracted development compared to the cortical samples. This pattern was confirmed by the ROI analyses. Early maturation was seen in the pericalcarine (~14 years) and lateral occipital cortex (~19 years). Most protracted development was seen in frontal areas including caudal middle frontal (~27 years), lateral orbitofrontal (~29 years), medial orbitofrontal (~30 years), pars orbitalis (~31 years), and rostral middle frontal (~31 years). Prolonged development was also seen in temporal areas including entorhinal (~29 years), parahippocampal (~27 years), and superior temporal gyrus (~79 years). Subcortical WM T1-weighted signal intensity showed a slightly more protracted development compared to the intracortical GM signal intensity but still displayed the characteristic early maturational period followed by an accelerating decrease in middle adulthood and senescence. The effects of including R2* in the statistical models were stronger in the WM compared to the intracortical GM analyses in the youngest age group. Residual WM T1-weighted signal intensity increases were observed in medial and lateral anterior temporal and orbitofrontal areas. The effects of including cortical thickness as an additional vertexwise covariate were small across groups.

*Intracortical GM R2**

Supplementary Fig. 2 (right panel) shows statistical p maps ($p<.01$) from GLMs testing for quadratic effects of age on intracortical GM R2* while regressing out linear effects of age and sex. Strong negative quadratic effects (inversed U curves) of age were observed across the surface except in anterior temporal areas, the occipital poles, and parts of the orbitofrontal cortices. Results from multiple linear regressions with R2* as dependent and age, age^2, and sex as independent variables as well as peak estimations for various ROIs are summarized in Supplementary Table 1. Fig. 7 shows the rLOESS-estimated age trajectories for cortical GM R2* plotted with cortical thickness in eight neuroanatomical ROIs in the left hemisphere. In general, R2* showed stronger quadratic relations with age, peaked later than T1-weighted signal intensity and areas that showed no or

Table 2
Effects of sex, age, age^2, and ICV on intracortical GM T1-weighted signal intensity within various neuroanatomical ROIs in the left hemisphere.

	R^2	t_{sex}	t_{age}	t_{age^2}	t_{ICV}	Age at peak (rLOESS/OLS)
Banks sts	0.27	−0.14	2.66	**−4.94**	*3.44*	22.6/23.8
Caudal anterior cingulate	0.14	0.55	1.41	−2.79	3.02	22.8/20.0
Caudal middle frontal	0.17	−0.40	**3.83**	**−5.25**	*3.55*	27.8/30.6
Cuneus	0.40	−0.66	−0.82	−2.57	3.15	8.2/8.2
Entorhinal	0.18	0.39	2.13	*−3.52*	**4.53**	24.8/25.2
Fusiform	0.28	0.44	1.76	**−4.02**	**4.36**	21.5/17.8
Inferior parietal	0.29	−1.08	1.86	**−4.35**	*3.57*	13.7/19.2
Inferior temporal	0.22	0.02	1.54	*−3.51*	*3.74*	23.0/19.3
Isthmus cingulate	0.27	0.29	2.03	**−4.25**	**4.19**	18.8/18.8
Lateral occipital	0.36	−2.04	−0.44	−2.65	2.61	8.2/8.2
Lateral orbitofrontal	0.16	0.21	3.01	**−4.52**	2.45	26.6/27.8
Lingual	0.40	−0.36	0.40	*−3.69*	**4.16**	8.9/8.2
Medial orbitofrontal	0.20	0.28	2.45	**−4.26**	3.29	24.1/23.0
Middle temporal	0.20	−0.43	2.18	**−4.03**	*3.44*	24.1/23.7
Paracentral	0.26	−0.29	2.89	**−4.93**	**4.06**	22.8/24.5
Parahippocampal	0.29	0.75	0.86	−3.18	**4.74**	19.3/13.8
Pars opercularis	0.19	−0.47	3.11	**−4.75**	3.23	26.7/27.8
Pars orbitalis	0.11	−0.40	2.67	**−3.95**	1.86	27.8/28.4
Pars triangularis	0.20	−0.74	2.69	**−4.51**	2.82	26.0/26.6
Pericalcarine	0.46	−1.09	−1.09	−2.74	3.20	8.2/8.2
Postcentral	0.32	−0.80	2.29	**−4.94**	*3.60*	17.6/19.7
Posterior cingulate	0.23	0.48	1.70	*−3.67*	**4.02**	21.5/18.8
Precentral	0.23	−0.56	**4.82**	**−6.54**	*3.57*	27.3/30.5
Precuneus	0.33	−0.51	2.10	**−4.72**	**4.74**	15.9/18.8
Rostral anterior cingulate	0.13	0.55	0.36	−1.84	2.43	20.0/12.6
Rostral middle frontal	0.17	−0.19	2.98	**−4.65**	2.00	27.3/28.0
Superior frontal	0.11	−0.20	*3.78*	**−4.76**	2.87	28.8/34.0
Superior parietal	0.34	−1.18	1.87	**−4.66**	**4.15**	12.8/18.6
Superior temporal	0.26	−0.15	2.44	**−4.62**	**3.96**	22.8/21.9
Supramarginal	0.26	−0.44	2.86	**−5.03**	**3.83**	22.1/24.2

The parameters were estimated with linear regressions with signal intensity sampled at 1.0 mm into the cortex as dependent and sex, age, age^2, and ICV as independent variables. The right column denotes the age at rLOESS and OLS estimated peak for each ROI. R^2: adjusted R squared for the full model, t: t-score, bold: $p<.01$ (Bonferroni-corrected, factor of 60), italic/underlined: $p<.05$ (Bonferroni-corrected, factor of 60).

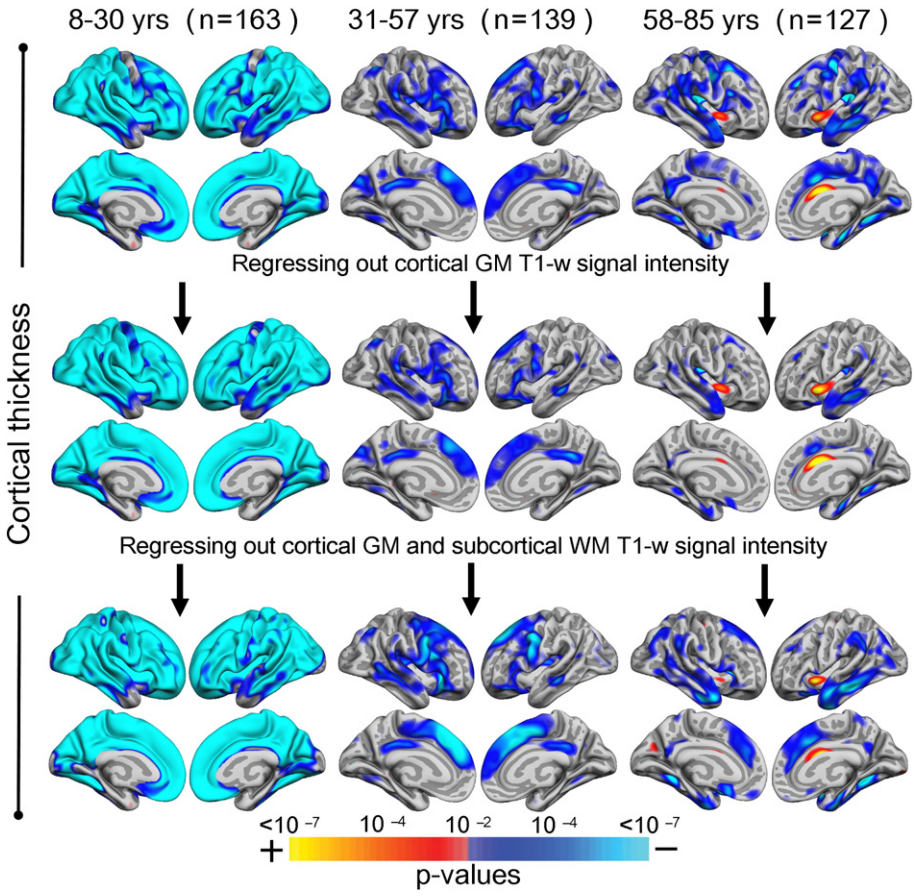

Fig. 4. Age-related intracortical GM changes in different age groups. The maps show the spatial distribution of *p* values from GLMs testing the effects of age on thickness before (bottom row) and after including intracortical GM (middle row) and subcortical WM T1-weighted signal intensity (bottom row) as vertexwise covariates in three different age groups. The analyses are based on 163 (young), 139 (middle-aged), and 127 (elderly) subjects. The maps are thresholded at $p<.01$, which in all instances with effects was regarded more conservative than a 5% FDR.

small significant quadratic age effects (e.g., the inferior temporal gyrus) continued increasing until mid 60s. Earliest peaks were seen bilaterally in the lateral occipital gyrus (~45 years), and the latest peaks were seen in temporal areas including entorhinal, superior (~57 years), and inferior temporal gyrus (~60 years). Fig. 8 shows the spatial *p* distribution from the GLMs testing for linear effects of age on cortical GM R2* in three different age groups before (top rows) and after (bottom rows) including cortical thickness as a vertexwise covariate. As suggested by the rLOESS and linear regressions, strong positive associations with age were found in the youngest subgroup. Positive effects were also found in the middle-aged group, especially in the lateral and medial parietal lobes and in anterior temporal areas. However, in the oldest group, R2* showed negative associations with age, especially in the lateral parietal lobes. Including cortical thickness increased the age variance in the two youngest groups and slightly decreased the effects of age in the oldest group.

Discussion

Cortical thinning in development and aging are caused by different neurobiological processes, but this cannot be monitored *in vivo* by use of imaging-derived cortical thickness measures alone. Here, we show that signal intensity obtained from heavily T1-weighted MRI scans is a promising biomarker of cortical age-related changes. In contrast to cortical thickness, T1-weighted signal intensity showed nonmonotone relationships with age, with strong maturational increases, a relatively stable plateau in middle age followed by decreases in senescence. The effects were, in general, found to be independent of concurrent cortical thinning. Although similar patterns were found for cortical GM R2*, the age effects on MP-RAGE signal intensity were observed largely independent of concurrent alterations in R2*. The patterns of maturational development and age-related deterioration of the signal intensity measures were consistent with the notion of an anterior–posterior gradient of cerebral maturation (Gogtay et al., 2004; Shaw et al., 2008) but in contrast to the frontal vulnerability in aging reported in morphometry studies (Fjell et al., 2009; Head et al., 2004; Jernigan et al., 2001; Raz and Rodrigue, 2006; Salat et al., 2005). Although interpretations must be done with caution without histological data available, the signal intensity and thickness changes may be related to, e.g., degree of intracortical axonal myelination (Barbier et al., 2002; Clark et al., 1992; Koenig et al., 1990; Paus et al., 2001; Sowell et al., 2001) in combination with activity-dependent changes in synaptic density (Bourgeois and Rakic, 1993; Huttenlocher and Dabholkar, 1997; Rakic et al., 1994). However, it is likely that a vast array of concurrent cellular and noncellular processes interact at various rates across development and aging (Tau and Peterson, 2010), and a full appreciation of the life span cortical changes can probably not be obtained with imaging data alone.

Intracortical signal intensity increases in maturation were observed, approaching a plateau in the late 20s or early 30s. In contrast to the monotone cortical thinning, signal intensity showed a clear dissociation between maturational and aging-related processes, supporting the notion that the measures are sensitive to distinct neurobiological properties

Maturational cortical thinning may be explained by use-dependent elimination of synaptic contacts (Bourgeois and Rakic, 1993;

Huttenlocher and Dabholkar, 1997; Rakic et al., 1994) with concurrent reduction in glial cells (Paus et al., 2008). Also, myelination of the peripheral neuropil could interact with the MRI contrast, yielding an *apparent* thinning of the cortex due to altered signal intensity and subsequent tissue misclassifications (Sowell et al., 2001). Signal intensity sampled from the MP-RAGE sequence is positively correlated with the underlying 1/T1 relaxation rates, resulting in T1 reduction in neurodevelopment (Barkovich, 2000; Paus et al., 2001; Steen et al., 1997; Steen and Schroeder, 2003) and T1 increase in aging (Agartz et al., 1991). As is the case for morphometry, the biological foundations for age-related changes in proton relaxation times are not sufficiently understood. Candidate mechanisms include alterations of the structure and density of axonal myelin (Koenig et al., 1990; Laule et al., 2007; Paus et al., 2001), bioaccumulation of iron depositions (Ogg and Steen, 1998), and altered water content, possibly modulated by neuronal loss and altered synaptic density. Due to proton–lipid interactions, increased myelination is expected to increase T1 relaxation rates (Sigalovsky et al., 2006) and thus also T1-weighted signal intensity sampled from MP-RAGE scans. Increased water concentration, which may be related to myelin, synaptic, and axonal deterioration, decreases T1-weighted signal intensity. Myelin-related changes in aged monkeys have been reported (Peters, 2002), including accumulating water compartments in the myelin sheaths (Feldman and Peters, 1998), formation of redundant myelin, splitting of the myelin lamellae, and loss of myelinated fibers (Marner et al., 2003; Sandell and Peters, 2003).

Although the obtained MRI signal is a weighted sum of various cellular, axonal, and other properties, it has been shown that a high degree of myelination results in stronger T1 MRI signal (Barbier et al., 2002; Clark et al., 1992). This is supported by studies comparing MRI with spatially corresponding myelin-stained sections suggesting that most of the signal is derived from myelin (Walters et al., 2003), and that cortical T1-weighted signal intensity is more similar to the myelo- than to the cytoarchitectonic profile of the tissue (Eickhoff et al., 2005).

Small-diameter fibers close to the cortical surface may be particularly prone to age-related breakdown (Marner et al., 2003), with strongest vulnerability in late-myelinating intracortical areas (Bartzokis, 2004). However, the patterns of age-related signal intensity alterations do not provide ample evidence for a simple first-in-last-out hypothesis (Raz, 2000). While superior frontal areas were latest to fully mature, as indexed by signal intensity, these were not among the first to decline with age. Cortical GM signal intensity reductions were most significant in posterior parietal and occipital regions in the oldest group. This stands in contrast to the frontally distributed cortical thinning seen in the present study as well as previous reports of increased aging-related vulnerability of the frontal lobes (Fjell et al., 2009; Raz and Rodrigue, 2006). Thus, a simple frontal aging hypothesis may not fit well when considering multimodal data in concert (Westlye et al., in press). This is also in line with a recent prospective DTI study, which found no evidence of accelerated frontal decline during a 2-year period in adults aged 50–90 years (Barrick et al., 2010).

The timing of maximum signal intensity roughly corresponded to the age where regional decelerating thinning was seen. The concurrent decelerating thinning and signal intensity peaks could reflect a maturational milestone in cortical development. The

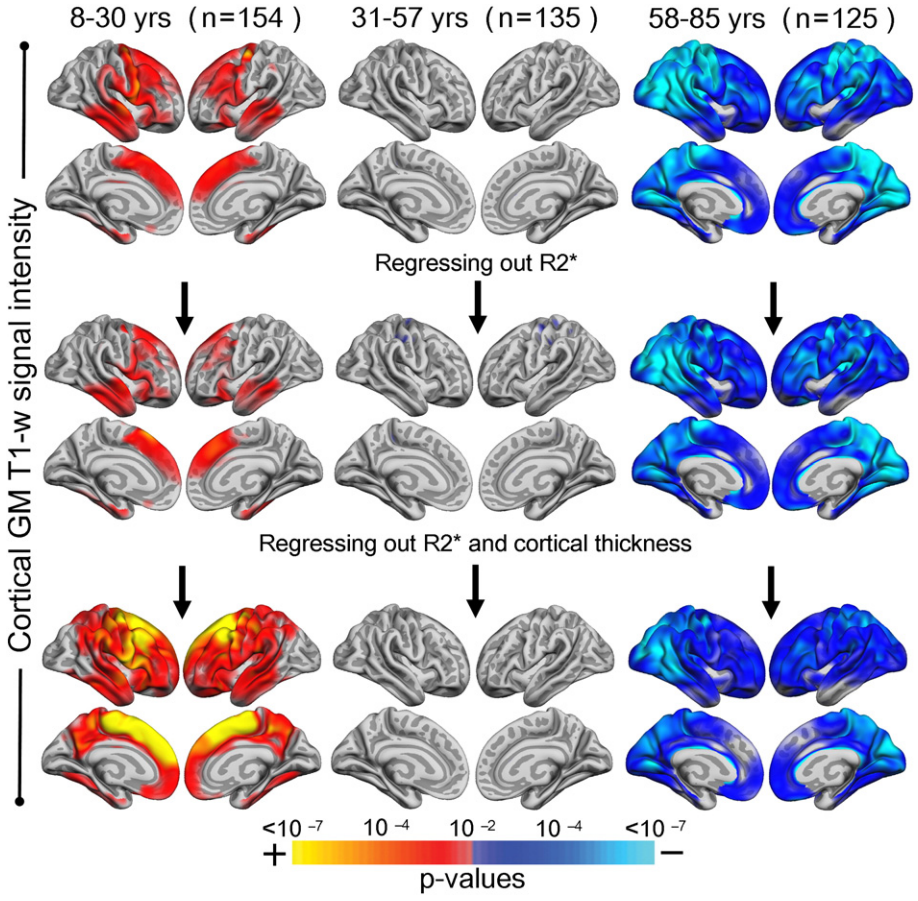

Fig. 5. Age-related intracortical GM changes in different age groups. The maps show the spatial *p* distribution from GLMs testing the effects of age on intracortical GM signal intensity before (top row) and after including cortical R2* (middle row) and cortical thickness (bottom row) as vertexwise covariates (bottom rows), respectively, in three different age groups. The analyses are based on 154 (young), 135 (middle-aged), and 125 (elderly) subjects. The maps are thresholded at $p < .01$, which in all instances with effects was regarded more conservative than a 5% FDR.

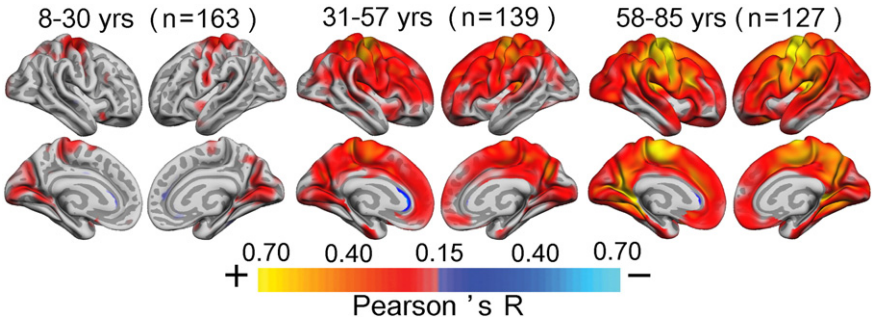

Fig. 6. Vertexwise correlations between cortical thickness and intracortical GM signal intensity. Warm colors denote positive correlations. The correlations (Pearson's *R*) between measures increase with age. The surface maps are thresholded at $R>.15$ and color-coded (see color bar). The signal intensity values were residualized for ICV before the analysis.

correlations between thickness and signal intensity were weak in development but positive and increasing in strength with age. Whether the stronger positive correlation in the oldest groups is due to biology or imperfections in cortical measurement techniques remains a topic of further research. In either case, these results support the view that the relations between the different cortical GM measures are not uniform across the life span. Further research utilising multimodal data is needed to explore the dynamic relations between cortical thickness and signal intensity and also to track the functional correlates of the different measures.

In addition to the effects of altered levels and structure of myelin and synaptic density, it has been proposed that T1-weighted signal intensity alterations are driven by bioaccumulated iron (Ogg and Steen, 1998; Paus et al., 1999). About 90% of nonheme cerebral iron is deposited in the iron storage protein ferritin (Bartzokis et al., 1997) which exerts strong magnetic effects resulting in shortening of T2 and T2* relaxation rates. Changes in T2 and T2* relaxation modulate the T1-weighted signal intensity, even on strongly T1-weighted acquisitions like the MP-RAGE sequence used in the present study. Elevated iron concentrations have been observed in normal aging (Stankiewicz et al., 2007) and may contribute to myelin susceptibility (Bartzokis, 2004). Protracted maturational T2 alterations may persist into the third decade of life (Hassink et al., 1992) and quantitative relaxation studies have shown age-related alterations in T2 and T2* relaxation (Bartzokis et al., 1997; Bartzokis et al., 2004; Péran et al., 2007; Siemonsen et al., 2008). Our analyses showed that although cortical GM R2* showed strong age-related variability, including R2* in the statistical models only to a minor extent influenced estimated age effects on intracortical GM MP-RAGE signal intensity. The observed changes in MP-RAGE signal intensity may thus be mainly explained by

Table 3
Effects of sex, age, age^2, and ICV on subcortical WM T1-weighted signal intensity within various neuroanatomical ROIs in the left hemisphere.

	R^2	t_{sex}	t_{age}	t_{age^2}	t_{ICV}	Peak (rLOESS/OLS)
Banks sts	0.21	0.69	3.02	**−4.84**	2.75	24.5/27.3
Caudal anterior cingulate	0.19	2.17	0.54	−2.32	2.31	19.3/8.2
Caudal middle frontal	0.18	1.04	*3.41*	**−4.87**	2.85	27.3/28.8
Cuneus	0.19	0.40	1.61	−3.24	*3.75*	19.3/20.0
Entorhinal	0.22	2.11	**5.77**	**−6.59**	**4.55**	29.1/36.0
Fusiform	0.28	1.07	**4.13**	**−6.11**	**4.40**	25.2/28.1
Inferior parietal	0.21	0.24	3.25	**−5.01**	3.34	23.3/27.3
Inferior temporal	0.23	0.64	*3.72*	**−5.50**	*3.69*	26.0/28.8
Isthmus cingulate	0.25	0.95	1.35	*−3.41*	**3.96**	14.5/13.7
Lateral occipital	0.20	−0.94	0.90	−2.95	2.54	19.0/17.3
Lateral orbitofrontal	0.16	0.74	**4.48**	**−5.73**	2.83	28.8/33.0
Lingual	0.24	0.49	2.69	**−4.50**	**4.75**	23.1/24.8
Medial orbitofrontal	0.19	1.34	**4.77**	**−5.96**	*3.73*	29.8/34.0
Middle temporal	0.22	0.38	**4.27**	**−5.93**	*3.56*	26.6/30.5
Paracentral	0.20	1.50	2.00	*−3.69*	*3.39*	26.6/21.9
Parahippocampal	0.18	1.08	**4.45**	**−5.34**	**4.86**	27.3/33.0
Pars opercularis	0.18	0.27	3.15	**−4.70**	3.24	26.6/28.1
Pars orbitalis	0.11	0.30	**4.75**	**−5.53**	2.24	30.8/36.0
Pars triangularis	0.14	−0.05	*3.42*	**−4.74**	2.55	27.8/29.8
Pericalcarine	0.25	−0.03	0.39	−2.67	*3.39*	13.6/9.8
Postcentral	0.18	0.53	*3.55*	**−4.86**	**4.07**	26.6/29.1
Posterior cingulate	0.22	1.62	0.95	−2.80	*3.45*	17.0/8.2
Precentral	0.19	1.17	2.13	**−3.83**	2.93	24.5/23.5
Precuneus	0.24	0.85	**3.89**	**−5.55**	**4.53**	26.0/29.8
Rostral anterior cingulate	0.17	1.61	0.76	−2.49	1.70	17.3/14.0
Rostral middle frontal	0.14	0.61	**4.24**	**−5.36**	2.49	30.5/33.0
Superior frontal	0.16	0.99	**4.21**	**−5.48**	2.71	28.8/32.0
Superior parietal	0.20	0.32	**4.08**	**−5.58**	**3.94**	27.8/31.0
Superior temporal	0.20	0.32	**4.19**	**−5.60**	**4.14**	27.3/31.0
Supramarginal	0.20	0.93	**4.05**	**−5.48**	*3.79*	27.3/30.8

The parameters were estimated with linear regressions with signal intensity sampled at 2.0 mm into the subcortical WM as dependent and sex, age, age^2, and ICV as independent variables. The right column denotes the age at rLOESS and OLS estimated peak for each ROI. R^2: adjusted *R* squared for the full model, *t*: *t*-score, bold: $p<.01$ (Bonferroni-corrected, factor of 60), italic/underlined: $p<.05$ (Bonferroni-corrected, factor of 60).

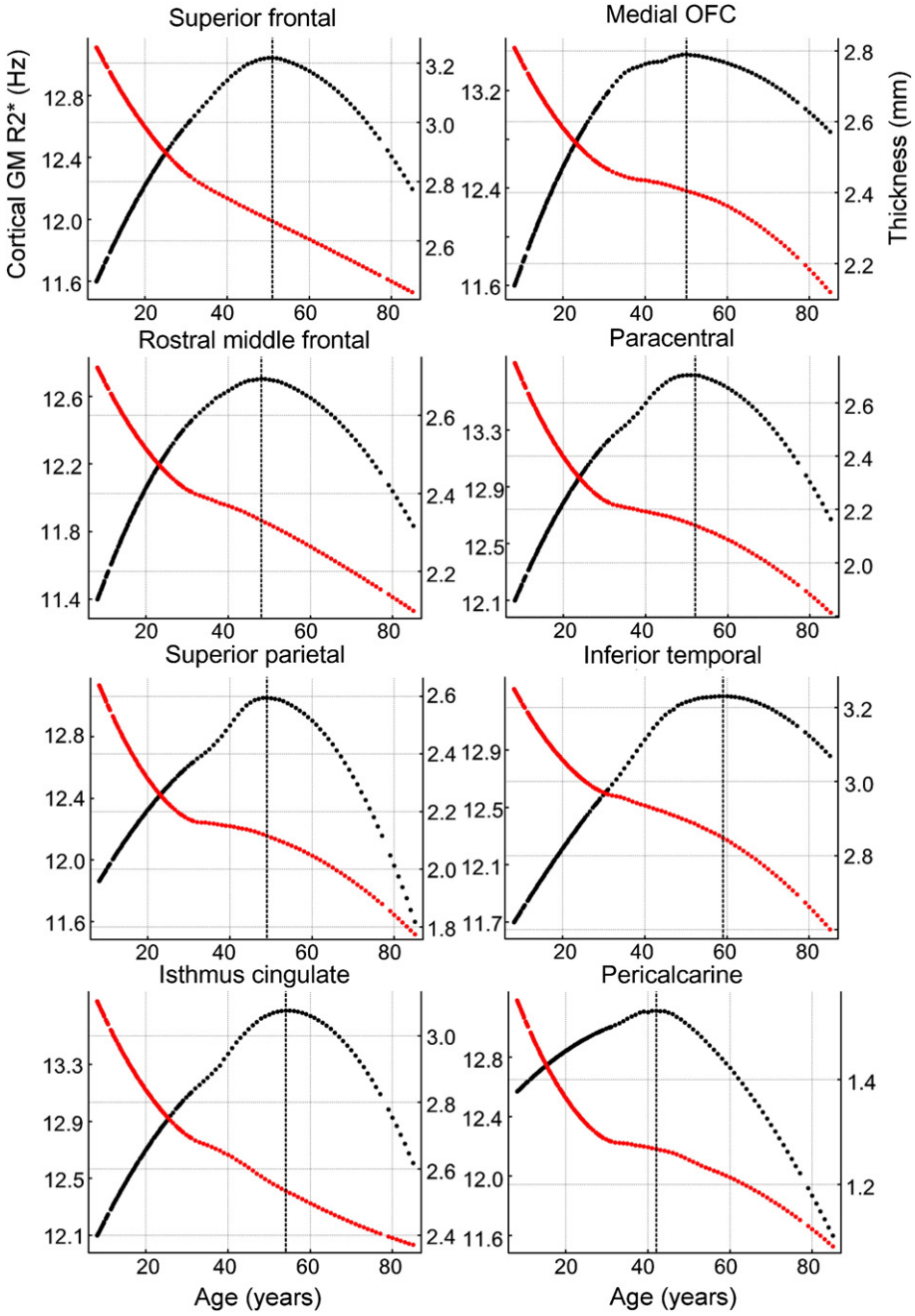

Fig. 7. Intracortical GM R2* through the life span. rLOESS estimated curves for cortical GM R2* (black dots) and cortical thickness (red dots) in select ROIs plotted as a function of age. The left *y*-axes denote the R2* and the right *y*-axes denote the cortical thickness (mm). The vertical dotted lines mark the rLOESS-estimated peaks of cortical GM R2*.

biophysical changes in T1 relaxation rates rather than R2* changes secondary to tissue iron content.

A potential caveat is that the cortical surface and the lateral ventricles used as reference are distal in terms of B0 and B1, and this may have influenced the results. For the main analyses, we did not correct for intensity nonuniformity, which could interact with head size and thus possibly age and sex. However, our analyses revealed strong correlations between signal intensity values sampled from corrected and noncorrected volumes. Also, except for less clear maturational signal intensity increases in the superior frontal gyrus and the isthmus cingulate in values sampled from the nonuniformity corrected volumes, the rLOESS-estimated age trajectories were very similar across measures. Further, the linear regressions showed strong unique quadratic age effects also when including ICV, age, and sex as covariates. All surface-based analyses were performed on the residuals of the signal intensity maps after removing ICV-related variance on a vertex-by-vertex manner. Thus, age^2 exerted strong effects independent of concurrent alterations in ICV. Further, direct comparisons of the age trajectories between the nonuniformity corrected and the noncorrected volumes yielded highly similar curves. The vertexwise correlations between the surface mapped values were also high across the surface. Thus, we do not think that sampling MP-RAGE intensity values from nonuniformity corrected volumes would substantially alter the results in the current data set. However, further research should explore possible influences of various normalization procedures on

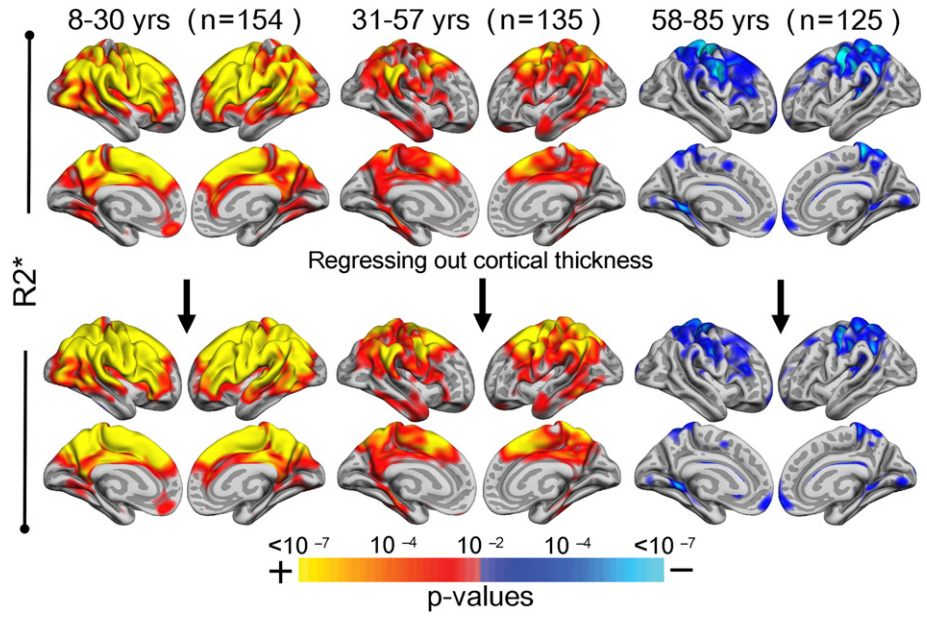

Fig. 8. Linear effects of age on intracortical GM R2* in different age groups. The figure shows statistical *p* maps from GLMs testing the effects of age on intracortical GM R2* before (top row) and after (bottom row) regressing out cortical thickness in three different age groups. The analyses are based on 154 (young group), 135 (middle-aged group), and 125 (elderly group) subjects. The *p* maps are thresholded at $p<.01$ (uncorrected). The medial wall including corpus callosum is masked.

the age effects and also possible interactions with field strength and other scanner-related parameters.

A possible common explanatory factor for the observed thickness and signal intensity changes in neurodevelopment is that tissue boundary segmentation become more accurate as myelination progresses. This could lead to shifts in the GM/WM tissue boundaries influencing apparent thickness and signal intensity measures (Westlye et al., 2009b). In the present study, we found strong age-related alterations of both intracortical GM and subjacent WM signal intensity. Future research should be aimed at exploring the relationship between cortical thickness and various intrinsic cortical GM and WM MRI properties (Sigalovsky et al., 2006). Further studies on the biophysical properties of the MRI parameters are needed, and the results from the current cross-sectional study should be elaborated with longitudinal data and clinical groups and also by including subjects younger than eight years of age. Individual differences in normal maturational and adult cortical trajectories are likely modulated by various complex genetic (Kremen et al., 2010; Panizzon et al., 2009) and environmental interactions (Boyke et al., 2008; Draganski et al., 2004; Driemeyer et al., 2008; Raz and Rodrigue, 2006; Sowell et al., 2008), and future studies may succeed in incorporating and isolating the effects of such modulating variables.

Conclusively, in contrast to the monotone decrease in cortical thickness observed from eight years of age, the course of the intracortical GM and subcortical WM T1-weighted signal intensity followed an inverted U shape with opposite effects seen in development and aging. The results yielded spatially distinct age-related patterns in the earliest and latest parts of life, in line with the view that the neurobiological mechanisms for thinning of the cerebral cortex are different in development versus aging. The famous first-in-last-out hypothesis was not supported, in that prefrontal areas did not show selective decreases in signal intensity in aging, even though their development was prolonged. Intracortical GM signal intensity alterations were seen largely independent of concurrent cortical thinning and accumulation of cerebral iron, leaving age-related alterations of intracortical/neuropil myelination and synaptic density as two core candidates for the observed effects. The supplemental information provided by T1-weighted signal intensity and R2* to cortical thickness suggests that these measures may provide highly valuable biomarkers in the study of neurodevelopment, healthy aging and possibly disease.

Disclosure statement

Anders M. Dale is a founder and holds equity in CorTechs Labs, Inc, and also serves on the Scientific Advisory Board. The terms of this arrangement have been reviewed and approved by the University of California, San Diego, in accordance with its conflict of interest policies. All other authors state that there are no actual or potential conflicts of interest. Appropriate approval and procedures were used concerning human subjects participating in the study.

Acknowledgments

This study was supported by the Norwegian Research Council (grant 177404/W50 to K.B.W. and 175066/D15 to A.M.F.) and the University of Oslo to K.B.W. and A.M.F. The authors wish to express their gratitude to three anonymous reviewers for constructive comments on an earlier version of the article.

Appendix A. Supplementary data

Supplementary data associated with this article can be found, in the online version, at doi:10.1016/j.neuroimage.2010.03.056.

References

Agartz, I., Saaf, J., Wahlund, L.O., Wetterberg, L., 1991. T1 and T2 relaxation time estimates in the normal human brain. Radiology 181, 537–543.

Barbier, E.L., Marrett, S., Danek, A., Vortmeyer, A., van Gelderen, P., Duyn, J., Bandettini, P., Grafman, J., Koretsky, A.P., 2002. Imaging cortical anatomy by high-resolution MR at 3.0 T: detection of the stripe of Gennari in visual area 17. Magn. Reson. Med. 48, 735–738.

Barkovich, A.J., 2000. Concepts of myelin and myelination in neuroradiology. AJNR Am. J. Neuroradiol. 21, 1099–1109.

Barrick, T.R., Charlton, R., Clark, C.A., Markus, H.S., 2010. White matter structural decline in normal ageing: a prospective longitudinal study using tract-based spatial statistics. Neuroimage 51 (2), 565–577.

Bartzokis, G., 2004. Age-related myelin breakdown: a developmental model of cognitive decline and Alzheimer's disease. Neurobiol. Aging 25, 5–18 author reply 49–62.
Bartzokis, G., Beckson, M., Hance, D.B., Marx, P., Foster, J.A., Marder, S.R., 1997. MR evaluation of age-related increase of brain iron in young adult and older normal males. Magn. Reson. Imaging 15, 29–35.
Bartzokis, G., Sultzer, D., Lu, P.H., Nuechterlein, K.H., Mintz, J., Cummings, J.L., 2004. Heterogeneous age-related breakdown of white matter structural integrity: implications for cortical "disconnection" in aging and Alzheimer's disease. Neurobiol. Aging 25, 843–851.
Beck, A.T., Steer, R., 1987. Beck Depression Inventory Scoring Manual. The Psychological Corporation, New York.
Bertoni-Freddari, C., Fattoretti, P., Delfino, A., Solazzi, M., Giorgetti, B., Ulrich, J., Meier-Ruge, W., 2002. Deafferentative synaptopathology in physiological aging and Alzheimer's disease. Ann. N.Y. Acad. Sci. 977, 322–326.
Bourgeois, J.P., Rakic, P., 1993. Changes of synaptic density in the primary visual cortex of the macaque monkey from fetal to adult stage. J. Neurosci. 13, 2801–2820.
Boyke, J., Driemeyer, J., Gaser, C., Buchel, C., May, A., 2008. Training-induced brain structure changes in the elderly. J. Neurosci. 28, 7031–7035.
Buckner, R.L., Head, D., Parker, J., Fotenos, A.F., Marcus, D., Morris, J.C., Snyder, A.Z., 2004. A unified approach for morphometric and functional data analysis in young, old, and demented adults using automated atlas-based head size normalization: reliability and validation against manual measurement of total intracranial volume. Neuroimage 23, 724–738.
Clark, V.P., Courchesne, E., Grafe, M., 1992. In vivo myeloarchitectonic analysis of human striate and extrastriate cortex using magnetic resonance imaging. Cereb. Cortex 2, 417–424.
Cleveland, W.S., Devlin, S.J., 1988. Locally weighted regression: an approach to regression analysis by local fitting. J. Am. Stat. Assoc. 83, 596–610.
Courchesne, E., Chisum, H.J., Townsend, J., Cowles, A., Covington, J., Egaas, B., Harwood, M., Hinds, S., Press, G.A., 2000. Normal brain development and aging: quantitative analysis at in vivo MR imaging in healthy volunteers. Radiology 216, 672–682.
Dale, A.M., Fischl, B., Sereno, M.I., 1999. Cortical surface-based analysis: I. Segmentation and surface reconstruction. Neuroimage 9, 179–194.
Dale, A.M., Sereno, M.I., 1993. Improved localization of cortical activity by combining EEG and MEG with MRI cortical surface reconstruction: a linear approach. J. Cogn. Neurosci. 5, 162–176.
Desikan, R.S., Segonne, F., Fischl, B., Quinn, B.T., Dickerson, B.C., Blacker, D., Buckner, R.L., Dale, A.M., Maguire, R.P., Hyman, B.T., Albert, M.S., Killiany, R.J., 2006. An automated labeling system for subdividing the human cerebral cortex on MRI scans into gyral based regions of interest. Neuroimage 31, 968–980.
Draganski, B., Gaser, C., Busch, V., Schuierer, G., Bogdahn, U., May, A., 2004. Neuroplasticity: changes in grey matter induced by training. Nature 427, 311–312.
Driemeyer, J., Boyke, J., Gaser, C., Buchel, C., May, A., 2008. Changes in gray matter induced by learning—revisited. PLoS ONE 3, e2669.
Eickhoff, S., Walters, N.B., Schleicher, A., Kril, J., Egan, G.F., Zilles, K., Watson, J.D., Amunts, K., 2005. High-resolution MRI reflects myeloarchitecture and cytoarchitecture of human cerebral cortex. Hum. Brain Mapp. 24, 206–215.
Feldman, M.L., Peters, A., 1998. Ballooning of myelin sheaths in normally aged macaques. J. Neurocytol. 27, 605–614.
Fischl, B., Dale, A.M., 2000. Measuring the thickness of the human cerebral cortex from magnetic resonance images. Proc. Nat. Acad. Sci. U.S.A. 97, 11050–11055.
Fischl, B., Salat, D.H., Busa, E., Albert, M., Dieterich, M., Haselgrove, C., van der Kouwe, A., Killiany, R., Kennedy, D., Klaveness, S., Montillo, A., Makris, N., Rosen, B., Dale, A.M., 2002. Whole brain segmentation: automated labeling of neuroanatomical structures in the human brain. Neuron 33, 341–355.
Fischl, B., Salat, D.H., van der Kouwe, A.J., Makris, N., Segonne, F., Quinn, B.T., Dale, A.M., 2004a. Sequence-independent segmentation of magnetic resonance images. Neuroimage 23 (Suppl 1), S69–S84.
Fischl, B., Sereno, M.I., Dale, A.M., 1999a. Cortical surface-based analysis: II. Inflation, flattening, and a surface-based coordinate system. Neuroimage 9, 195–207.
Fischl, B., Sereno, M.I., Tootell, R.B., Dale, A.M., 1999b. High-resolution intersubject averaging and a coordinate system for the cortical surface. Hum. Brain Mapp. 8, 272–284.
Fischl, B., van der Kouwe, A., Destrieux, C., Halgren, E., Segonne, F., Salat, D.H., Busa, E., Seidman, L.J., Goldstein, J., Kennedy, D., Caviness, V., Makris, N., Rosen, B., Dale, A.M., 2004b. Automatically parcellating the human cerebral cortex. Cereb. Cortex 14, 11–22.
Fjell, A.M., Westlye, L.T., Amlien, I., Espeseth, T., Reinvang, I., Raz, N., Agartz, I., Salat, D.H., Greve, D.N., Fischl, B., Dale, A.M., Walhovd, K.B., 2009. High consistency of regional cortical thinning in aging across multiple samples. Cereb. Cortex 19, 2001–2012.
Folstein, M.F., Folstein, S.E., McHugh, P.R., 1975. Mini-mental state. A practical method for grading the cognitive state of patients for the clinician. J. Psychiatr. Res. 12, 189–198.
Genovese, C.R., Lazar, N.A., Nichols, T., 2002. Thresholding of statistical maps in functional neuroimaging using the false discovery rate. Neuroimage 15, 870–878.
Giedd, J.N., Blumenthal, J., Jeffries, N.O., Castellanos, F.X., Liu, H., Zijdenbos, A., Paus, T., Evans, A.C., Rapoport, J.L., 1999. Brain development during childhood and adolescence: a longitudinal MRI study. Nat. Neurosci. 2, 861–863.
Gogtay, N., Giedd, J.N., Lusk, L., Hayashi, K.M., Greenstein, D., Vaituzis, A.C., Nugent 3rd, T.F., Herman, D.H., Clasen, L.S., Toga, A.W., Rapoport, J.L., Thompson, P.M., 2004. Dynamic mapping of human cortical development during childhood through early adulthood. Proc. Natl. Acad. Sci. U.S.A. 101, 8174–8179.
Good, C.D., Johnsrude, I.S., Ashburner, J., Henson, R.N., Friston, K.J., Frackowiak, R.S., 2001. A voxel-based morphometric study of ageing in 465 normal adult human brains. Neuroimage 14, 21–36.
Greve, D.N., Fischl, B., 2009. Accurate and robust brain image alignment using boundary-based registration. Neuroimage 48, 63–72.
Han, X., Fischl, B., 2007. Atlas renormalization for improved brain MR image segmentation across scanner platforms. IEEE Trans. Med. Imaging 26, 479–486.
Hassink, R.I., Hiltbrunner, B., Muller, S., Lutschg, J., 1992. Assessment of brain maturation by T2-weighted MRI. Neuropediatrics 23, 72–74.
Head, D., Buckner, R.L., Shimony, J.S., Williams, L.E., Akbudak, E., Conturo, T.E., McAvoy, M., Morris, J.C., Snyder, A.Z., 2004. Differential vulnerability of anterior white matter in nondemented aging with minimal acceleration in dementia of the Alzheimer type: evidence from diffusion tensor imaging. Cereb. Cortex 14, 410–423.
Huttenlocher, P.R., Dabholkar, A.S., 1997. Regional differences in synaptogenesis in human cerebral cortex. J. Comp. Neurol. 387, 167–178.
Jernigan, T.L., Archibald, S.L., Fennema-Notestine, C., Gamst, A.C., Stout, J.C., Bonner, J., Hesselink, J.R., 2001. Effects of age on tissues and regions of the cerebrum and cerebellum. Neurobiol. Aging 22, 581–594.
Koenig, S.H., Brown 3rd, R.D., Spiller, M., Lundbom, N., 1990. Relaxometry of brain: why white matter appears bright in MRI. Magn. Reson. Med. 14, 482–495.
Kremen, W.S., Prom-Wormley, E., Panizzon, M.S., Eyler, L.T., Fischl, B., Neale, M.C., Franz, C.E., Lyons, M.J., Pacheco, J., Perry, M.E., Stevens, A., Schmitt, J.E., Grant, M. D., Seidman, L.J., Thermenos, H.W., Tsuang, M.T., Eisen, S.A., Dale, A.M., Fennema-Notestine, C., 2010. Genetic and environmental influences on the size of specific brain regions in midlife: the VETSA MRI study. Neuroimage 49, 1213–1223.
Kuperberg, G.R., Broome, M.R., McGuire, P.K., David, A.S., Eddy, M., Ozawa, F., Goff, D., West, W.C., Williams, S.C., van der Kouwe, A.J., Salat, D.H., Dale, A.M., Fischl, B., 2003. Regionally localized thinning of the cerebral cortex in schizophrenia. Arch. Gen. Psychiatry 60, 878–888.
Laule, C., Vavasour, I.M., Kolind, S.H., Li, D.K., Traboulsee, T.L., Moore, G.R., MacKay, A.L., 2007. Magnetic resonance imaging of myelin. Neurotherapeutics 4, 460–484.
Lebel, C., Walker, L., Leemans, A., Phillips, L., Beaulieu, C., 2008. Microstructural maturation of the human brain from childhood to adulthood. Neuroimage 40, 1044–1055.
Marner, L., Nyengaard, J.R., Tang, Y., Pakkenberg, B., 2003. Marked loss of myelinated nerve fibers in the human brain with age. J. Comp. Neurol. 462, 144–152.
Morrison, J.H., Hof, P.R., 1997. Life and death of neurons in the aging brain. Science 278, 412–419.
Nairn, J.G., Bedi, K.S., Mayhew, T.M., Campbell, L.F., 1989. On the number of Purkinje cells in the human cerebellum: unbiased estimates obtained by using the "fractionator". J. Comp. Neurol. 290, 527–532.
Ogg, R.J., Steen, R.G., 1998. Age-related changes in brain T1 are correlated with iron concentration. Magn. Reson. Med. 40, 749–753.
Panizzon, M.S., Fennema-Notestine, C., Eyler, L.T., Jernigan, T.L., Prom-Wormley, E., Neale, M., Jacobson, K., Lyons, M.J., Grant, M.D., Franz, C.E., Xian, H., Tsuang, M., Fischl, B., Seidman, L., Dale, A., Kremen, W.S., 2009. Distinct genetic influences on cortical surface area and cortical thickness. Cereb. Cortex 19, 2728–2735.
Paus, T., Collins, D.L., Evans, A.C., Leonard, G., Pike, B., Zijdenbos, A., 2001. Maturation of white matter in the human brain: a review of magnetic resonance studies. Brain Res. Bull. 54, 255–266.
Paus, T., Keshavan, M., Giedd, J.N., 2008. Why do many psychiatric disorders emerge during adolescence? Nat. Rev. Neurosci. 9, 947–957.
Paus, T., Zijdenbos, A., Worsley, K., Collins, D.L., Blumenthal, J., Giedd, J.N., Rapoport, J.L., Evans, A.C., 1999. Structural maturation of neural pathways in children and adolescents: in vivo study. Science 283, 1908–1911.
Péran, P., Hagberg, G., Luccichenti, G., Cherubini, A., Brainovich, V., Celsis, P., Caltagirone, C., Sabatini, U., 2007. Voxel-based analysis of R2* maps in the healthy human brain. J. Magn. Reson. Imaging 26, 1413–1420.
Peters, A., 2002. Structural changes that occur during normal aging of primate cerebral hemispheres. Neurosci. Biobehav. Rev. 26, 733–741.
Rakic, P., Bourgeois, J.P., Goldman-Rakic, P.S., 1994. Synaptic development of the cerebral cortex: implications for learning, memory, and mental illness. Prog. Brain Res. 102, 227–243.
Raz, N., 2000. Aging of the brain and its impact on cognitive performance: integration of structural and functional findings. In: Craik, F.I.M., Salthouse, T.A. (Eds.), Handbook of Aging and Cognition - II. Erlbaum, Mahwah, NJ, pp. 1–90.
Raz, N., Gunning-Dixon, F., Head, D., Rodrigue, K.M., Williamson, A., Acker, J.D., 2004. Aging, sexual dimorphism, and hemispheric asymmetry of the cerebral cortex: replicability of regional differences in volume. Neurobiol. Aging 25, 377–396.
Raz, N., Rodrigue, K.M., 2006. Differential aging of the brain: patterns, cognitive correlates and modifiers. Neurosci. Biobehav. Rev. 30, 730–748.
Rosas, H.D., Liu, A.K., Hersch, S., Glessner, M., Ferrante, R.J., Salat, D.H., van der Kouwe, A., Jenkins, B.G., Dale, A.M., Fischl, B., 2002. Regional and progressive thinning of the cortical ribbon in Huntington's disease. Neurology 58, 695–701.
Salat, D.H., Buckner, R.L., Snyder, A.Z., Greve, D.N., Desikan, R.S., Busa, E., Morris, J.C., Dale, A.M., Fischl, B., 2004. Thinning of the cerebral cortex in aging. Cereb. Cortex 14, 721–730.
Salat, D.H., Lee, S.Y., van der Kouwe, A.J., Greve, D.N., Fischl, B., Rosas, H.D., 2009. Age-associated alterations in cortical gray and white matter signal intensity and gray to white matter contrast. Neuroimage 48, 21–28.
Salat, D.H., Tuch, D.S., Hevelone, N.D., Fischl, B., Corkin, S., Rosas, H.D., Dale, A.M., 2005. Age-related changes in prefrontal white matter measured by diffusion tensor imaging. Ann. N.Y. Acad. Sci. 1064, 37–49.
Sandell, J.H., Peters, A., 2003. Disrupted myelin and axon loss in the anterior commissure of the aged rhesus monkey. J. Comp. Neurol. 466, 14–30.
Shaw, P., Kabani, N.J., Lerch, J.P., Eckstrand, K., Lenroot, R., Gogtay, N., Greenstein, D., Clasen, L., Evans, A., Rapoport, J.L., Giedd, J.N., Wise, S.P., 2008. Neurodevelopmental trajectories of the human cerebral cortex. J. Neurosci. 28, 3586–3594.

Siemonsen, S., Finsterbusch, J., Matschke, J., Lorenzen, A., Ding, X.Q., Fiehler, J., 2008. Age-dependent normal values of T2* and T2′ in brain parenchyma. AJNR Am. J. Neuroradiol. 29, 950–955.
Sigalovsky, I.S., Fischl, B., Melcher, J.R., 2006. Mapping an intrinsic MR property of gray matter in auditory cortex of living humans: a possible marker for primary cortex and hemispheric differences. Neuroimage 32, 1524–1537.
Sled, J.G., Zijdenbos, A.P., Evans, A.C., 1998. A nonparametric method for automatic correction of intensity nonuniformity in MRI data. IEEE Trans. Med. Imaging 17, 87–97.
Sowell, E.R., Mattson, S.N., Kan, E., Thompson, P.M., Riley, E.P., Toga, A.W., 2008. Abnormal cortical thickness and brain–behavior correlation patterns in individuals with heavy prenatal alcohol exposure. Cereb. Cortex 18, 136–144.
Sowell, E.R., Peterson, B.S., Thompson, P.M., Welcome, S.E., Henkenius, A.L., Toga, A.W., 2003. Mapping cortical change across the human life span. Nat. Neurosci. 6, 309–315.
Sowell, E.R., Thompson, P.M., Leonard, C.M., Welcome, S.E., Kan, E., Toga, A.W., 2004. Longitudinal mapping of cortical thickness and brain growth in normal children. J. Neurosci. 24, 8223–8231.
Sowell, E.R., Thompson, P.M., Tessner, K.D., Toga, A.W., 2001. Mapping continued brain growth and gray matter density reduction in dorsal frontal cortex: inverse relationships during postadolescent brain maturation. J. Neurosci. 21, 8819–8829.
Stankiewicz, J., Panter, S.S., Neema, M., Arora, A., Batt, C.E., Bakshi, R., 2007. Iron in chronic brain disorders: imaging and neurotherapeutic implications. Neurotherapeutics 4, 371–386.
Steen, R.G., Ogg, R.J., Reddick, W.E., Kingsley, P.B., 1997. Age-related changes in the pediatric brain: quantitative MR evidence of maturational changes during adolescence. AJNR Am. J. Neuroradiol. 18, 819–828.
Steen, R.G., Schroeder, J., 2003. Age-related changes in the pediatric brain: proton T1 in healthy children and in children with sickle cell disease. Magn. Reson. Imaging 21, 9–15.
Tamnes, C.K., Østby, Y., Fjell, A.M., Westlye, L.T., Due-Tønnessen, P., Walhovd, K.B., 2010. Brain maturation in adolescence and young adulthood: regional age-related changes in cortical thickness and white matter volume and microstructure. Cereb Cortex. 20, 534–548.
Tau, G.Z., Peterson, B.S., 2010. Normal development of brain circuits. Neuropsychopharmacology 35, 147–168.
Terry, R.D., DeTeresa, R., Hansen, L.A., 1987. Neocortical cell counts in normal human adult aging. Ann. Neurol. 21, 530–539.
Walters, N.B., Egan, G.F., Kril, J.J., Kean, M., Waley, P., Jenkinson, M., Watson, J.D., 2003. In vivo identification of human cortical areas using high-resolution MRI: an approach to cerebral structure–function correlation. Proc. Natl. Acad. Sci. U.S.A. 100, 2981–2986.
Wechsler, D., 1999. Wechsler Abbreviated Scale of Intelligence. The Psychological Corporation, San Antonio, TX.
Westlye, L.T., Walhovd, K.B., Bjørnerud, A., Due-Tønnessen, P., Fjell, A.M., 2009a. Error-related negativity is mediated by fractional anisotropy in the posterior cingulate gyrus—a study combining diffusion tensor imaging and electrophysiology in healthy adults. Cereb. Cortex 19, 293–304.
Westlye, L.T., Walhovd, K.B., Dale, A.M., Bjørnerud, A., Due-Tønnessen, P., Engvig, A., Grydeland, H., Tamnes, C.K., Østby, Y., Fjell, A.M., in press. Life-span changes of the human brain white matter: diffusion tensor imaging (DTI) and volumetry. Cereb Cortex. http://dx.doi.org/10.1093/cercor/bhp280.
Westlye, L.T., Walhovd, K.B., Dale, A.M., Espeseth, T., Reinvang, I., Raz, N., Agartz, I., Greve, D.N., Fischl, B., Fjell, A.M., 2009b. Increased sensitivity to effects of normal aging and Alzheimer's disease on cortical thickness by adjustment for local variability in gray/white contrast: a multi-sample MRI study. Neuroimage 47, 1545–1557.
Yakovlev, P., Lecours, A., 1967. The myelogenetic cycles of regional maturation of the brain. In: Minkowski, A. (Ed.), Regional Development of the Brain in Early Life. Blackwell, Oxford, pp. 3–70.